

Unimorph piezoelectric deformable mirrors for space telescopes

P. Rausch, S. Verpoort, U. Wittrock
Photonics Laboratory, Muenster University of Applied Sciences
Stegerwaldstraße 39, 48565 Steinfurt, Germany

ABSTRACT

We have developed, manufactured and tested a unimorph deformable mirror for space applications based on piezoelectric actuation. The mirror was designed for the correction of low-order Zernike modes with a stroke of several tens of micrometers over a clear aperture of 50 mm. It was successfully tested in thermal vacuum, underwent lifetime tests, and was exposed to random vibrations, sinusoidal vibrations, and to ionizing radiation. We report on design considerations, manufacturing of the mirror, and present the test results. Furthermore, we discuss critical design parameters, and how our mirror could be adapted to serve recently proposed space telescopes such as HDST and TALC.

Keywords: Unimorph deformable mirror, space telescopes, piezoelectric actuation, environmental testing

1. INTRODUCTION

Space telescopes with large primary mirrors suffer from wavefront aberrations. The primary mirror's mass and size are ultimately limited by the constraints imposed by the launch vehicle, hence the design of space telescopes with large primary mirrors calls for structures that are lightweight and/or segmented. The conventional method to produce optics with high surface fidelity is precluded, since it relies on the use of thick mirror substrates which provide the rigidity needed to maintain the mirror's surface figure. A segmented primary allows larger apertures, but phasing and alignment of the individual segments is challenging and introduces another source of wave-front error. One key element in the implementation of large space telescope is active optics. Active optics allow for correction of wavefront errors induced by the static aberrations of a warped primary mirror, and for correction of aberrations which occur during operation, e.g. due to thermal stress. Additionally, the requirements on mechanical stability of the optical train are eased, thus reducing weight of the supporting structures. Active optics may also reduce the impact of wavefront errors caused by unpredicted surface distortions and alignment errors which would have to be corrected by costly servicing missions. The prime example being Hubble's flawed primary mirror.

In recent years, efforts have been made to develop lightweight primary mirrors that incorporate actuators which allow to actively control the mirror's surface figure¹⁻⁴. Another, more commonly used approach, uses a deformable mirror placed further down the optical train in a plane conjugate to the primary mirror⁵⁻¹⁰. The latter approach moves the complexity of active optics to scales where they are easier to manage: away from the large primary to a smaller mirror that needs less actuation force, has a higher temporal bandwidth, and operates in a thermally stable environment inside the telescope.

However, active shape control of primary mirrors would allow alternative manufacturing processes, which is important especially for segmented primaries. Grinding and polishing the individual mirror segments to the designated surface figure is costly and time-consuming. An alternative fabrication technique, which is comparably simple and of low cost, relies on replication of mirror segments from a master mold. However, the replication process is never perfect, hence the surface figure of the segments would have to be corrected afterwards. Actively controlled segments manufactured in a simple and low cost replication process are one key aspect to show the feasibility of very large segmented and lightweight space telescopes, such as TALC¹¹.

Under the GSTP activity "Development of Adaptive Deformable Mirrors for Space Instruments", funded by the European Space Agency, we have developed, manufactured and tested a space-qualified unimorph deformable mirror¹²⁻¹⁴. The goal was a generic technology development for a deformable mirror that would be used in a plane conjugate to the primary mirror of a large space telescope. ESA had called for a mirror that had to generate low order Zernike modes with a fairly large peak-to-valley (PV) surface stroke of 30 μm in defocus mode (60 μm PV wavefront), and 5 μm PV surface stroke in trefoil mode over a clear aperture of 50 mm. The modes had to be produced with a residual RMS

surface error below 30 nm. The mirror we developed can be readily adapted to suite different space telescopes. For example, the mirror could be made annular such that its deformation eigenmodes resemble that of a large monolithic primary mirror. For a telescope with a segmented primary, a segmented array of unimorph deformable mirrors could be designed, such that each segment of the primary mirror is imaged onto one unimorph deformable mirror. With additional piston and tip-tilt actuation, this array of unimorph mirrors could provide phasing and aberration correction of the segments of the primary mirror.

2. DESIGN

The active structure of our mirror is shown in Fig. 1. It consists of a piezoelectric disc (PIC 151 from PI Ceramic) with an overall diameter of 84 mm which is sandwiched between two metallic electrodes. The disc is subdivided by laser-cutting into a central disc with a diameter of 64 mm, and three arms. The electrode on the back side of the central disc is structured into a 44-electrode keystone pattern. A coated glass substrate (Schott N-BK10) with an overall diameter of 64 mm is bonded to the central disc with a space qualified 2-component epoxy (Epo-Tek 353ND), forming a laminate. We refer to this laminate as the “mirror structure”. The area of the mirror that can be controlled with high precision has a diameter of 50 mm and is marked by white dashed circles in Fig. 1. Due to the simple unimorph design, the mirror structures weighs only about 100 g. Since the mirror is based on just a few, precisely CTE-matched materials, it is insensitive to temperature variations.

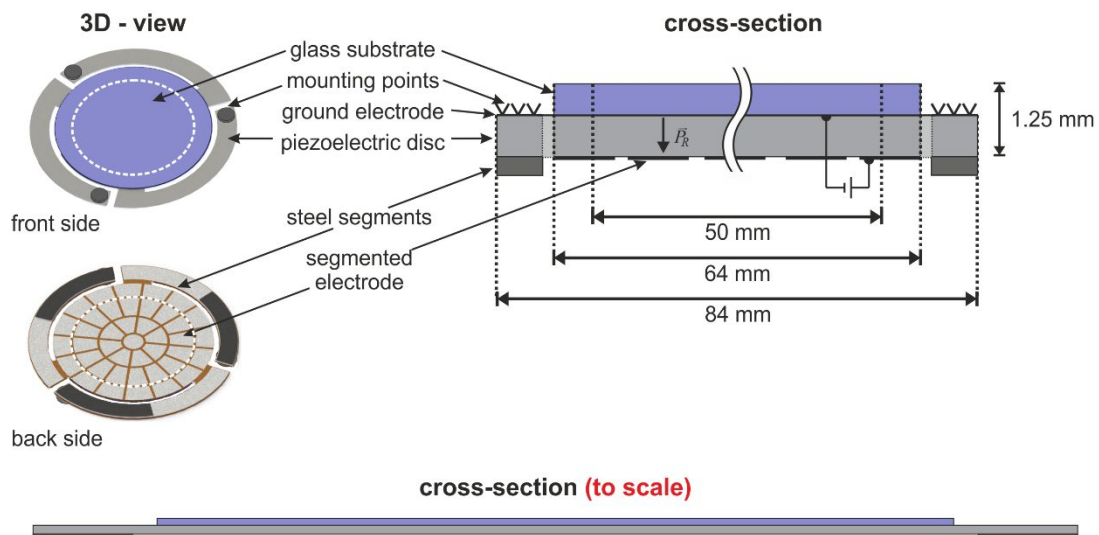


Figure 1. 3D-view of front side and back side of the mirror structure (left) along with a cross-sectional view (right). A cross-sectional view drawn to scale is shown at the bottom of the figure.

The mirror structure is firmly fixed to three support points via the three arms, providing high rigidity while allowing the central disc to deform almost freely. Steel segments are glued to the arms as a passive layer. In that way, the arms not only serve as mounting but enable an integrated, monolithic tip/tilt functionality without the need for additional equipment. We use the Fe-/Ni alloy Kovar (material number 1.3917) for the steel segments. The coefficient of thermal expansion (CTE) of Kovar is nearly matched with the CTE of the piezoelectric material PIC 151¹², avoiding thermally induced deformations of the three arms.

The electrode pattern on the back side has been optimized numerically to produce low order Zernike modes up to the 12th mode with large stroke (e.g. >40 μm in defocus mode, >10 μm in trefoil mode) and diffraction limited surface fidelity at 1 μm wavelength. Throughout this paper, we use the Zernike notation of Wyant and Creath¹⁵. A detailed view of the back side electrode pattern is shown in Fig. 2.

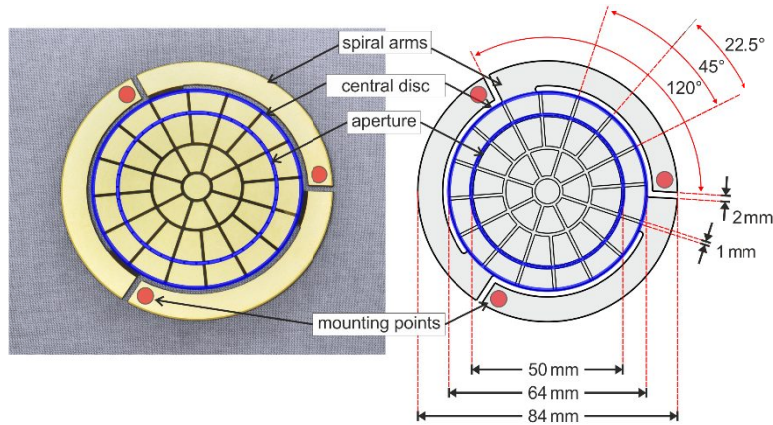


Figure 2. Details of the mirror's electrode pattern.

To mount the main mirror structure into the housing, the arms of the three-arm structure were glued onto a three-point mount which is also made of Kovar. We used an electrically conductive two-component epoxy (Epo-Tek 4110-LV) to ensure electrical connection between the ground electrode and the mounting structure. A photograph of the mounted mirror structure is shown in Fig. 3.

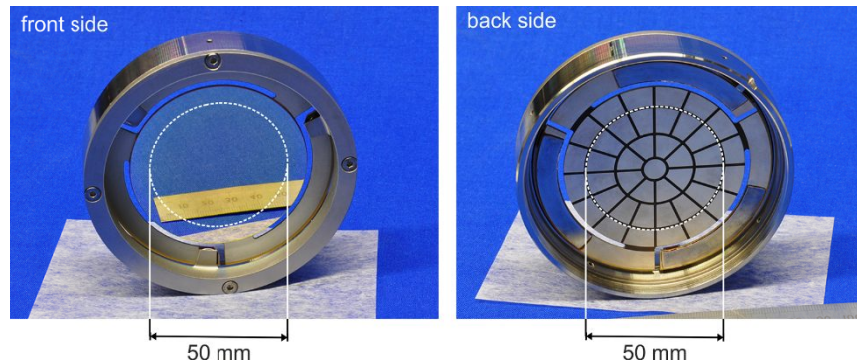


Figure 3. Front side and back side of the mounted mirror structure. The net aperture of 50 mm which is used to create designated surface figures is marked by a dashed circle.

An exploded view of the mirror assembly is shown on the left side of Fig. 4. All housing parts were made from Kovar to allow for large temperature variations without temperature-induced deformations. The circuit boards facilitating the electric connection were made from Al_2O_3 ceramics with screen-printed circuits. The back side electrodes on the piezo disc were connected to the "connection circuit board" via gold wires with a thickness of $25 \mu\text{m}$. The connection circuit board is connected to the "back panel circuit board" via plugs. The right side of Fig. 4 shows the fully assembled mirror, which fits in commercially available 4" mirror mounts.

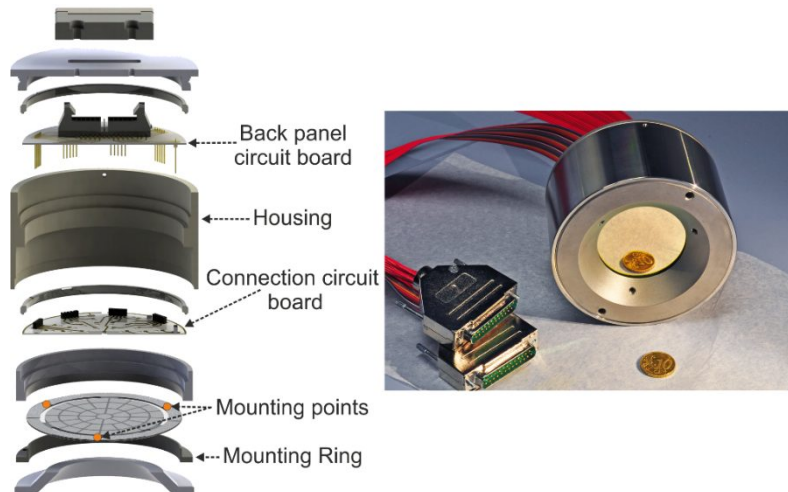


Figure 4. Assembly of the deformable mirror. a) exploded view. b) fully assembled mirror

3. CHARACTERIZATION

3.1 Measurement setup

The surface of the deformable mirror was characterized using a phase-shifting Twyman-Green interferometer. A schematic view of the whole measurement setup is shown in Fig. 5. Light from a Helium-Neon laser is spatially filtered with a microscope objective and a pinhole with a diameter of $25\ \mu\text{m}$. The emerging beam is collimated by lens L_1 to a diameter of approximately 20 mm and split into a reference arm and a measurement arm. In the measurement arm, the beam is expanded by a telescope comprised of the lenses L_2 and L_3 to a diameter of 75 mm and reflected by the deformable mirror. The light from the measurement arm and the reference arm is superimposed at the beam splitter, demagnified by a telescope comprised of the lenses L_4 and L_5 , and directed onto a camera. The surface of the deformable mirror and the surface of the camera chip lie in conjugated planes formed by the two telescopes.

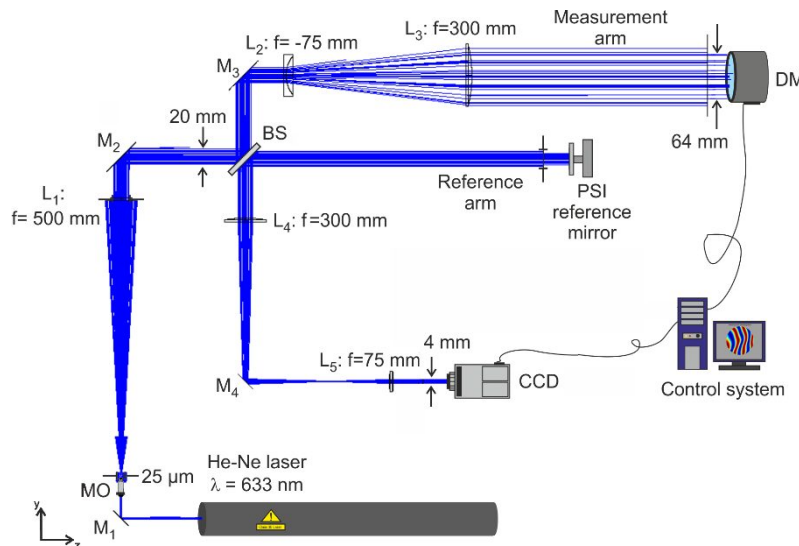


Figure 5. Surface measurement setup used to characterize the deformable mirror's surface. M: mirror, MO: microscope objective, L: lens, BS: beam splitter, DM: deformable mirror, SHS: Shack-Hartmann wavefront sensor.

The reference mirror is mounted onto a piezo stack to facilitate phase shifts between the reference arm and the measurement arm. Five interferograms are recorded, the phase shift between each interferogram is $\lambda/4$. The wrapped

phase profile is reconstructed from the five interferograms using a five-point Schwider-Hariharan algorithm¹⁶, the phase profile is unwrapped by means of quality-guided phase unwrapping¹⁷. The measurement setup has a repeatability of 2 nm RMS and an absolute PV accuracy of 10 nm.

3.2 Generation of Zernike modes

To characterize the possible surface shapes of the deformable mirror, the Zernike modes Z_1 to Z_{12} were produced in closed-loop operation to determine the maximum Zernike amplitudes and the respective surface fidelities. Exemplary interferograms of selected Zernike modes produced by the deformable mirror are shown in Fig. 6.

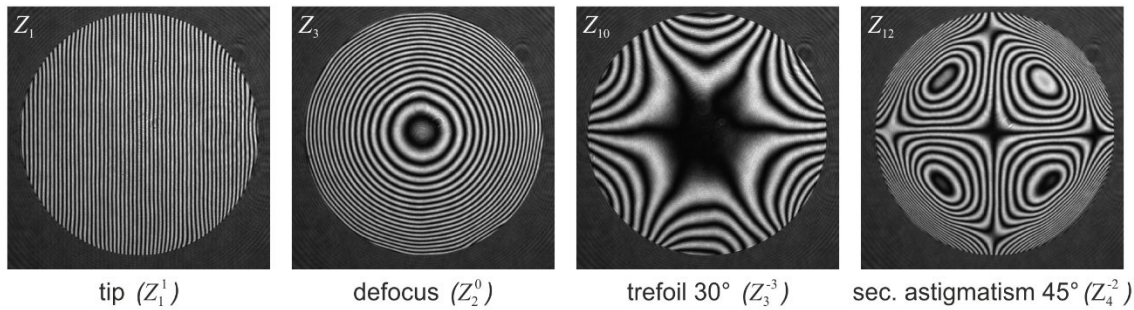


Figure 6. Interferograms of Zernike modes produced by the deformable mirror. The consecutive numbers shown in the upper left corner of each interferogram corresponds to the ordering used in¹⁴.

The PV surface amplitude of the Zernike mode that should be produced by the mirror was raised in steps of 0.5 μm until one of the following criteria arose: The measured residual RMS deviation from the target surface exceeded $\lambda/14$ ($\lambda = 1064 \text{ nm}$, Maréchal-criterion), or the required voltage exceeded the maximum allowed voltage of $\pm 400 \text{ V}$. The comparison between numerically calculated and measured maximum Zernike amplitudes is shown in Fig. 7 along with the surface stroke requirements from ESA. The measured amplitudes correspond well to the numerically calculated Zernike amplitudes. The strokes exceed ESA's requirements. In defocus mode (Z_3), a stroke of 45 μm was achieved (30 μm required), the trefoil modes ($Z_{9,10}$) were produced with a stroke of 15 μm (5 μm required).

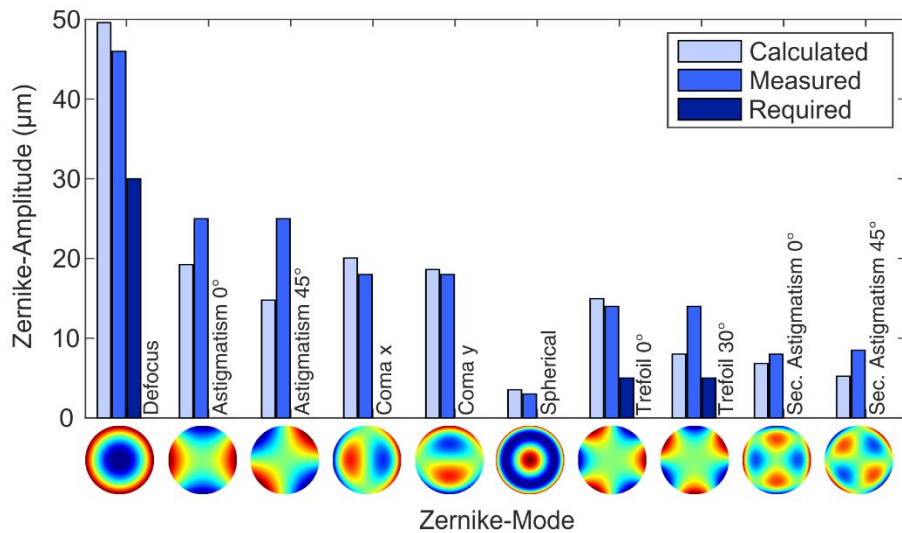


Figure 7. Comparison of numerically calculated and measured Zernike surface PV amplitudes. Each measured amplitude is either voltage or Maréchal limited

3.2 Mitigation of print-through

The surface figure of the deformable mirror can be separated into two parts. One part contains deformation of low order which can be compensated for by the deformable mirror. The main contribution to this low order aberration is typically

of astigmatic shape. The second part is comprised of deformations with higher order, which cannot be compensated for by the mirror.

High spatial frequency deformations caused by the actuators, commonly referred to as print-through, is a frequently encountered problem for deformable mirrors¹⁸⁻²⁰. Print-through is best observed if the mirror is actively flattened. The surface of the first deformable mirror generation in the actively flattened state is shown in Fig. 8 a). The resemblance of the residual surface deviation to the electrode pattern is apparent. In a recent paper¹³, we ascribed the development of print-through in unimorph deformable mirrors to piezoelectric domain reorientation, a term also referred to as “poling strain”³. The residual surface deviation from best sphere of the first mirror generation was 40 nm RMS, the main contribution originates from print-through. By suitable pre-treatment of the piezoelectric material and careful control of the manufacturing procedure, we were able to eliminate print-through to a level below 13 nm in the current generation, as shown in Fig. 8 c). The mitigation of print-through is a prerequisite to develop a unimorph mirror with very large stroke and high surface quality at the same time.

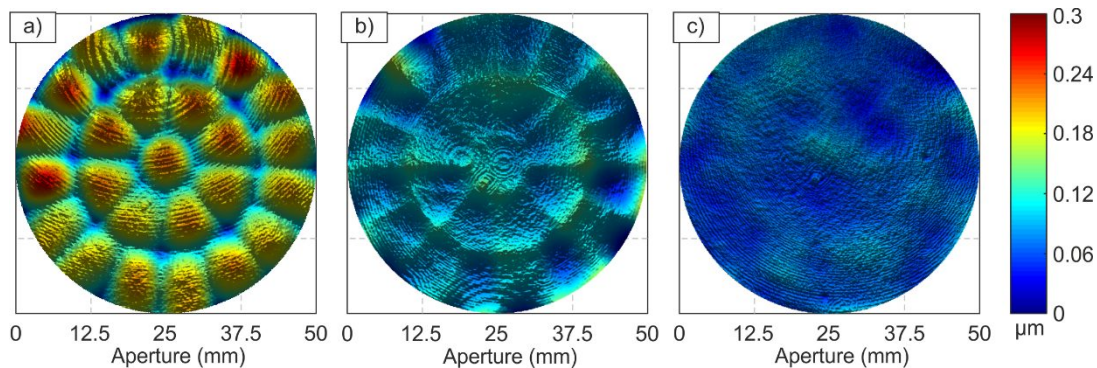


Figure 8. From left to right: residual surface deviation from best sphere of three successively manufactured deformable mirrors. **a)** First mirror generation, exhibiting a residual deviation from best sphere of 40 nm RMS. **b)** second mirror generation. The improved handling of the piezoelectric disc allowed for a residual deviation of 17 nm RMS. **c)** Current mirror generation. The residual deviation from best sphere is 13 nm RMS. The distinct electrode print-through is no longer visible.

4. ENVIRONMENTAL TESTING

Environmental tests were performed to assess the mirror’s compliance with space environment¹⁴. The mirror was operated in thermal vacuum, underwent a lifetime test, and was exposed to random vibrations, sinusoidal vibrations, and to ionizing and laser irradiation.

4.1 Thermal vacuum

To determine the deformable mirror’s performance at cryogenic temperatures, the mirror was operated at 300 K, 200 K, and 100 K inside a vacuum chamber at EADS Astrium. After operation at 100 K, the mirror was cycled 8 times between 100 K and 300 K. After the cycling, one final measurement was conducted. The mirror’s surface was measured from outside the vacuum chamber using a high resolution Shack-Hartmann wavefront sensor (Optocraft WFS SHS Lab 130-GE-UHR) with 116 x 116 lenslets.

Figure 9 depicts the maximum Zernike surface PV amplitudes obtained at the various temperatures. As can be seen, the mirror was operating successfully at all temperatures. The maximum Zernike amplitudes decrease with decreasing temperature. Compared to the amplitudes achieved at room temperature, the amplitudes dropped to 64 % ± 10 % at 200 K and 39 % ± 8 % at 100 K. This was expected, since the piezoelectric coefficients also decrease with decreasing temperature²¹. The decrease in stroke could be compensated for by using higher control voltages since the breakdown voltage of the piezoelectric material increases with decreasing temperature.

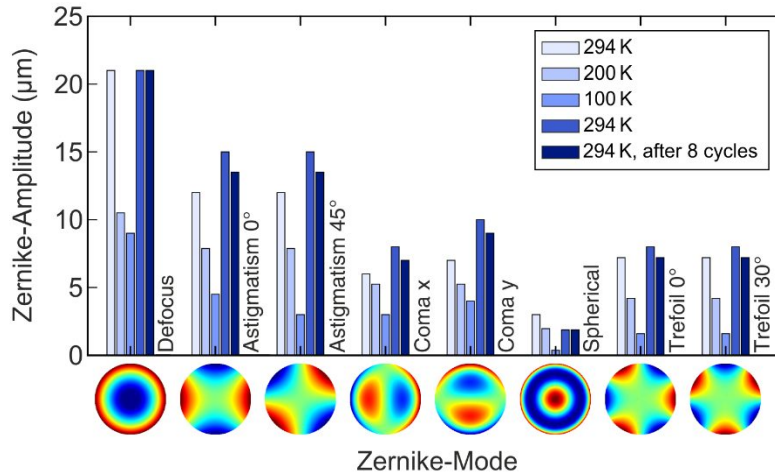


Figure 9. Maximum achieved Zernike surface PV amplitudes in thermal vacuum at different temperatures. The last test was conducted after eight thermal cycles between 100 K and 300 K

4.2 Vibrations

Vibration tests have been conducted to assess the mirrors resistance towards random and sine vibrations imposed by the launch vehicle. The demanded vibration levels are given in table 1. Due to the mirror's nearly cylindrical symmetry, vibration loads were applied in two directions. The directions are defined by the orientation of the reflective mirror surface. The direction perpendicular to the mirror surface is marked by the symbol “ \perp ”, the directions parallel to the mirror surface are marked by \parallel .

Table 1. Vibration test levels

Type	Frequency (Hz)	Sweep rate/slope	Vibration spectrum	Final level/Duration
Sine vibration (All directions)	5-21 21-60 60-100	2 Oct/min	-	11 mm (0 – peak) 20 g (0 – peak) 6 g (0 – peak)
Random vibration (\parallel)	20-100 100-400 400-2000	3.0 dB/Oct 0.0 dB/Oct -3.0 dB/Oct	(0.06 – 0.2) g^2/Hz 0.2 g^2/Hz (0.2 – 0.01) g^2/Hz	14.1 g RMS, 120 s
Random vibration (\perp)	20-100 100-400 400-2000	3.0 dB/Oct 0.0 dB/Oct -3.0 dB/Oct	(0.06 – 0.35) g^2/Hz 0.35 g^2/Hz (0.35 – 0.01) g^2/Hz	18.6 g RMS, 120 s

Two designs of the mirror structure were tested to assess the mirrors resistance towards vibrations: the “spiral arm” design and the “bridge” design. Both designs are depicted in Fig. 10. In the bridge design, the ends of the three spiral arms are connected to the junction of the next arm, forming a closed outer ring. This increases the stiffness of the mirror structure. Since the monolithic tip/tilt functionality is facilitated via unimorph actuation of the arms, the tip/tilt amplitudes of mirrors fabricated in the bridge design are reduced by approximately 50 %. The measured and calculated frequency response of the two designs due to excitation in the direction perpendicular to the mirror surface are shown in Fig. 11. As can be seen, stiffening the mirror structure by using the bridge lead to an almost three times higher frequency of the first Eigenmode. Increasing the first Eigenfrequency is beneficial in terms of increasing the mirrors resistance towards vibrations, since the mechanical stress due to excitation of an Eigenmode is proportional to the frequency of this Eigenmode²².

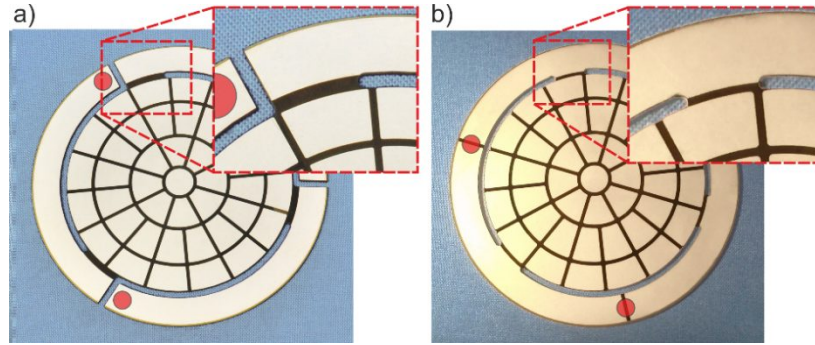


Figure 10. Detailed view of the two designs tested for vibrations. **a)** Spiral arm design. **b)** Bridge design. The insets show the junctions between the central disc and one of the arms in detail.

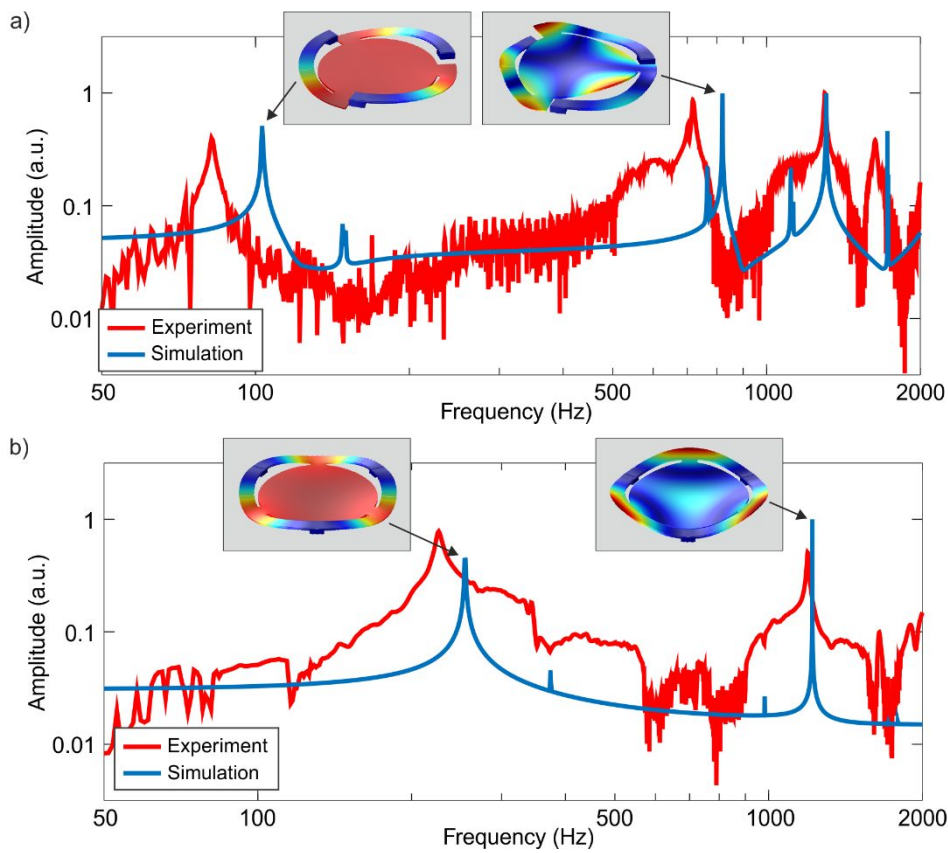


Figure 11. Measured (red) and calculated (blue) frequency response of the two mirror designs. **a)** Spiral arm design. **b)** Bridge design. The insets show the calculated shape of the first two dominant Eigenmodes of each design.

A summary of the conducted vibration tests is shown in table 2. For better readability, only the maximum tested levels are shown in the table. The deformable mirror with the bridge design passed the sine vibration tests in both vibration directions, as well as the random vibration test in a direction parallel to the mirror surface at full levels. Its structure broke at 50 % of the random vibration in the direction perpendicular to the mirror surface.

As can be inferred from the results, the simple yet effective structural modification that distinguishes the spiral arm design from the bridge design significantly increased the mirror's resistance towards vibrations.

Table 2. Summary of the vibration test results

Design	Sine vibration ()	Random vibration ()	Sine vibration (⊥)	Random vibration (⊥)
Spiral arm, 700 μm	20 g	14.1 g RMS	-	-
Bridge, 700 μm	20 g	14.1 g RMS	20 g	9.3 g RMS

The most recent design iteration has been further optimized to provide increased resistance towards vibrations by shifting the first Eigenfrequency from 250 Hz for the tested design to about 600 Hz. This should render the mirror compliant to common launch vehicles.

4.3 Ionizing irradiation, laser irradiation, and operation life time

The deformable mirror was subjected to gamma irradiation at ESTEC's Co60-facility. A total dose of 50 krad (Si) at a dose rate of 1 krad/h was used, the test was conducted at atmospheric pressure and room temperature.

Proton irradiation was carried out at the Proton Irradiation Facility (PIF) of the Paul-Scherrer Institute (PSI, Switzerland). The proton energy was adjusted to 30 MeV, approximately 29.75 MeV were incident on the optical surface due to the Kapton protection tape in front of the mirror surface. The proton flux was kept constant around $7 \cdot 10^6$ p⁺/s/cm². The total integrated fluence was $1 \cdot 10^{11}$ p⁺/cm². To assess the influence of different fluences, half of the mirror aperture was covered by a 10 mm thick aluminium plate to block a fluence of $0.5 \cdot 10^{11}$ p⁺/cm² (~50 % of the total fluence).

The laser power handling capability was tested with high pulse power (6 J/cm²) as well as with high average power (100 W, 1400 W/cm²). Three distinct spots on the mirror surface were irradiated.

The operation lifetime was assessed by applying a sinusoidal voltage signal with an amplitude of 350 V to all electrodes over a duration of 11 million full cycles.

The mirror performance prior and after each test was assessed by applying a voltage of 100 V to every actuator and measuring the PV amplitude of the actuator response. The ratio of the actuator responses from after and before the respective test is shown in Fig. 12. As can be seen, every actuator is still working. A drop of the response of actuator 43 to

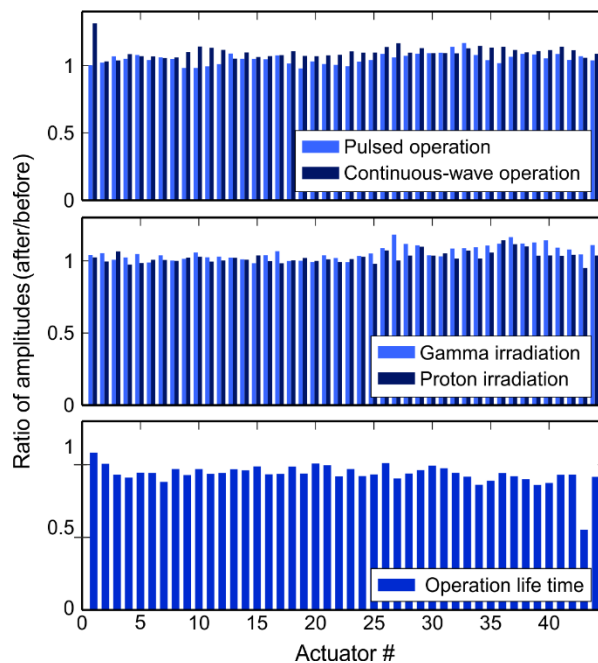


Figure 12. Measured ratios of the surface PV responses of each actuator for a voltage of 100 V prior and after the laser irradiation, ionizing irradiation, and operation life time test, respectively.

55 % of the initial value was observed after the operation life time test. Subsequent investigation revealed an increase of the electrical resistance of the actuator connection from approximately 5Ω to a few $M\Omega$. After the connection was reestablished using electrically conductive epoxy, the actuator response increased to 90 %.

5. CONCLUSION

We have developed, manufactured, and tested a unimorph deformable mirror for space applications based on piezoelectric actuation. The thin mirror structure can produce low order Zernike modes with a phase stroke of tens of micrometers. During the mirror development, we were able to reduce the mirror's high order residual deviation from best sphere to 13 nm RMS by mitigation of print-through, thus allowing for large stroke and high surface fidelity at the same time. Albeit allowing for large stroke, piezoelectric materials show hysteresis and creep. To obtain nanometer precision in producing a specific surface shape, the mirror should be embedded in a closed loop control scheme.

The conducted environmental tests have shown that the mirror is able to operate in space environment. This offers the possibility to utilize this technology on a future large space telescope. A deformable mirror could be used as a dedicated wavefront corrector down the optical train. The unimorph correction scheme is also suitable for active control of primary mirror segments. Manufacturing individual mirror segments is costly and time-consuming. An alternative strategy could involve the fast and repeatable fabrication of mirror segments by using replication techniques. Deviations from the surface figure due to manufacturing errors, gravity release, and thermal stress induced by CTE mismatch could be compensated for by embedding attaching active elements onto the mirror segments.

ACKNOWLEDGMENTS

The authors gratefully acknowledge support for the work presented by the European Space Agency under contract number 4000104030/10/NL/EM.

REFERENCES

- [1] G. Hickey, T. Barbee, M. Ealey, and D. Redding, "Actuated hybrid mirrors for space telescopes," *Proc. SPIE* 7731, 773120 (2010).
- [2] L. Gambicorti, F. D'Amato, F. Lisi, A. Riccardi, C. Vettore, F. Duo, A. Guercia, D. Gallieni, P. Lazzarini, M. Tintori, C. Patauner, R. Biasi, A. Zuccaro Marchi, and J. Pereira do Carmo, "Last results of technological developments for ultra-lightweight, large aperture, deployable mirror for space telescopes," in *Proceedings of the 9th International Conference on Space Optics (ICSO)*, Ajaccio, Corse (2012).
- [3] K. Patterson and S. Pellegrino, "Ultralightweight deformable mirrors," *Appl. Opt.* 52(22), 5327–5341 (2013).
- [4] Steeves, J., Laslandes, M., Pellegrino, S., Redding, D., Bradford, S. C., Wallace, J. K., & Barbee, T. "Design, fabrication and testing of active carbon shell mirrors for space telescope applications," *Proc. SPIE* 9151, 915105 (2014).
- [5] S. Manhart, W. J. Hupfer, S. Nikolov, C. Wuehrer, G. V. Vdovin, and Z. Sodnik, "50-mm MEMS deformable mirror," *Proc. SPIE* 4007, 555–562 (2000).
- [6] H. Dyson, R. Sharples, N. Dipper, G. Vdovin, "Cryogenic wavefront correction using membrane deformable mirrors," *Opt. Express* 8(1), 17–26, (2001).
- [7] M. A. Helmbrecht, T. Juneau, M. Hart, and N. Doble, "Segmented MEMS deformable-mirror technology for space applications," *Proc. SPIE* 6223, 622305 (2006).
- [8] J. B. Stewart, T. G. Bifano, S. Cornelissen, P. Bierden, B. M. Levine, and T. Cook, "Design and development of a 331-segment tip-tilt-piston mirror array for space-based adaptive optics," *Sensor. Actuat. A-Phys.* 138(1), 230–238 (2007).
- [9] M. Laslandes, E. Hugot, M. Ferrari, C. Hourtoule, C. Singer, C. Devilliers, C. Lopez, and F. Chazallet, "Mirror actively deformed and regulated for applications in space: design and performance," *Opt. Eng.* 52(9), 091803 (2013).
- [10] J.-C. Siquin, A. Bastard, E. Beaufort, T. Berkefeld, L. Cadiergues, V. Costes, R. Cousty, C. Dekhtiar, F. Di Gesu, X. Gilbert, C. Grezes-Besset, D. Groeninck, M. Hartung, H. Krol, A. Moreau, P. Morin, H. Pages, R. Palomo, G. Scharmer, D. Soltau, and J.-P. Veran, "Recent results and future DMs for astronomy and for space applications at CILAS," *Proc. SPIE* 9148, 91480G (2014).

- [11] G. Durand, M. Sauvage, A. Bonnet, L. Rodriguez, S. Ronayette, P. Chanial, L. Scola, V. Révéret, H. Aussel, M. Carty, et. al., "TALC: a new deployable concept for a 20 m far-infrared space telescope," Proc. SPIE 9143, 91431A (2014).
- [12] S. Verpoort, P. Rausch, and U. Wittrock, "Novel unimorph deformable mirror for space applications," in *Proceedings of the 9th International Conference on Space Optics (ICSO)*, Ajaccio, Corse (2012).
- [13] P. Rausch, S. Verpoort, and U. Wittrock, "Unimorph deformable mirror for space telescopes: design and manufacturing," Opt. Express 23(15), 19469-19477 (2015).
- [14] P. Rausch, S. Verpoort, and U. Wittrock, "Unimorph deformable mirror for space telescopes: environmental testing," Opt. Express 24(2), 1528-1542 (2016).
- [15] J.C. Wyant and K. Creath, "Basic wavefront aberration theory for optical metrology," in *Applied Optics and Optical Engineering*, Vol. XI, Chap. 1 (Academic, 1992).
- [16] P. Hariharan, B. F. Oreb, and T. Eiju, "Digital phase-shifting interferometry: a simple error-compensating phase calculation algorithm," Applied Optics 26(13), 2504-2506 (1987).
- [17] M. A. Herráez, D. R. Burton, M. J. Lalor, and M. A. Gdeisat, "Fast two-dimensional phase-unwrapping algorithm based on sorting by reliability following a noncontinuous path," Applied Optics 41(35), 7437-7444 (2002).
- [18] G. Cheriaux, J.-P. Rousseau, F. Burgy, J.-C. Siquin, J.-M. Lurçon, and C. Guillemard, "Monomorph large aperture adaptive optics for high peak-power femtosecond lasers," Proc. SPIE 6584, 658405 (2007).
- [19] J. Ma, Y. Liu, T. He, B. Li, and J. Chu, "Double drive modes unimorph deformable mirror for low-cost adaptive optics," Appl. Opt. 50(29), 5647-5654 (2011).
- [20] R. Bastait, D. Alaluf, M. Horodincea, I. Romanescu, I. Burda, G. Martic, G. Rodrigues, and A. Preumont, "Segmented bimorph mirrors for adaptive optics: segment design and experiment," Appl. Opt. 53(29), 6635-6642 (2014).
- [21] X. L. Zhang, Z. X. Chen, L. E. Cross, and W. A. Schulze, "Dielectric and piezoelectric properties of modified lead titanate zirconate ceramics from 4.2 to 300 K," J. Mater. Sci. 18(4), 968-972 (1983).
- [22] H. A. Gaberson and R. H. Chalmers, "Modal velocity as a criterion of shock severity," Shock and Vibration Bulletin 40(2), 31-49 (1969).